ELSEVIER

Carbohydrate Research 304 (1997) 303–314

CARBOHYDRATE RESEARCH

Conformation of cyclomaltooligosaccharide ("cycloamylose") of dp21 in aqueous solution

Shinichi Kitamura [a,*], Hiroshi Isuda [a], Jiro Shimada [b], Toshikazu Takada [b], Takeshi Takaha [c], Shigetaka Okada [c], Mitsuru Mimura [d], Kanji Kajiwara [d]

[a] *Department of Biological Resource Chemistry, Kyoto Prefectural University, Shimogamo, Kyoto 606, Japan*

[b] *Fundamental Research Laboratories, NEC, Miyukigaoka 34, Tsukuba, Ibaraki 305, Japan*

[c] *Biochemical Research Laboratory, Ezaki Glico, Utajima, Nishiyodogawa-ku, Osaka 555, Japan*

[d] *Faculty of Engineering and Design, Kyoto Institute of Technology, Matsugasaki, Kyoto 606, Japan*

Received 23 May 1997; accepted 6 August 1997

Abstract

The conformation of a cyclomaltooligosaccharide ["cycloamylose", cyclic (1 → 4)-α-D-glucan] having degree of polymerization 21 was characterized by means of small-angle X-ray scattering (SAXS) with the aid of simulations of scattering profile based on molecular models. The results indicate that the cycloamylose chains adopt a circularized three-turn single helical structure with a radius of gyration of 11.5 Å. The scattering profiles calculated for double helical structures with foldbacks at each end are not in good agreement with experimental profiles. Molecular dynamics simulations in water show that overall the conformation of the three-turn single-helical form is maintained at 300 K, although replacements of glucose units are observed. In one model, ninety-six water molecules are interacting with a cycloamylose molecule judging from hydrogen-bonding distances and angles.

Keywords: Cycloamylose; Small-angle X-ray scattering; Molecular modeling; Circularized single helical structure

1. Introduction

Cyclic (1 → 4)-α-D-glucans, (cyclomaltooligosaccharides, referred to as cycloamylose designated CA in this paper), are produced by action of D-enzyme [(1 → 4)-α-D-glucan:(1 → 4)α-D-glucan 4-α-D-glycosyltransferase, EC 2.4.1.25] on linear amylose [1]. The degree of polymerization (dp) of CA isolated from the reaction mixtures is found to range from 17 to several hundred. Thus the dp of CA is much larger than α-, the more common cyclomaltooligosaccharides, β-, and γ-cyclodextrins that have six, seven and eight sugar units, respectively.

CAs are expected to function as host molecules for many organic reagents and iodines [1] in a different manner from cyclodextrin since CAs may have a cavity geometry different from that of cyclodextrins.

* Corresponding author.

0008-6215/97/$17.00
PII S0008-6215(97)00278-4

Another interesting property of CAs is their high solubility in water, unlike linear amylose which is barely soluble in that solvent.

A conformational study of CA has been performed by computer modeling [2]. Two plausible conformations are proposed: the first is a circularized single-helical structure, and the second is a double-helical structure with foldbacks at each end. However, no experimental result is available for the conformation of CA in solution.

In this report, we describe the conformation of a CA with dp 21 (CA21) in aqueous solution as investigated by small-angle X-ray scattering (SAXS) and molecular modeling. The observed SAXS profiles were compared with those calculated directly from the atomic coordinates of the cyclic glucans generated by computer modeling. This method has been applied to linear oligosaccharides [3,4] and cyclosophoran [5] to give information on the conformation at the atomic level.

2. Materials and methods

Sample preparation.—CA mixtures were produced by the action of recombinant potato D-enzyme on synthetic amylose AS-320 (Nakano Vinegar, Aichi, Japan) as described previously [1]. About 500 mg of the mixtures thus obtained were size-fractionated by gel-filtration chromatography using a Superdex 30 column (26 × 500 mm, Pharmacia) with a flow rate of 2.5 mL/min. The fractions containing CAs with dp from 17 to 30 were collected and the glucans in the solution were recovered as a pellet by adding ten volumes of ethanol. Size-fractionated CA mixtures (25 mg) were loaded onto an ODS column (Daisopak SP-120-5-ODS-BP, 20 × 250 mm, Daiso, Osaka, Japan) and eluted with 6% (v/v) methanol with a flow rate of 9 mL/min. The glucan in the eluate was monitored by a refractive index detector (RID-6A, Shimadzu, Kyoto Japan), and the peak for CA21 was pooled, precipitated with ten volumes of ethanol, and then lyophilized. Purified CA21 showed a single peak on high-performance anion-exchange chromatography (HPAEC) with a Carbopac PA-100 column (4 × 250 mm, Dionex, CA). HPAEC was carried out with a Dionex DX-300 system with a pulsed amperometric detector (model PAD-II, Dionex) using the conditions described previously [1].

The molecular weight of CA21 was evaluated by the matrix-assisted laser-desorption time of flight spectroscopy (MALD–TOF). This technique has been previously applied for a CA mixture [1] and a cyclic hexadecaglucoside [6]. The samples were dissolved in 9:1 water–MeOH containing 100 mM 2,5-dihydroxybenzoic acid. Approximately 1 μL of this mixture was applied to a MALD probe and dried under vacuum. MALD–TOF spectra were recorded with a KOMPACT MALDI VI (Shimadzu/Kratos) spectrometer operating at 20 kV accelerating voltage.

NMR spectroscopy.—^{13}C NMR spectroscopy was performed with a JEOL 400 MHz spectrometer (LA 400) at 27.5 °C. All exchangeable H of the samples were substituted by D before obtaining the spectra in deuterium oxide. The sample concentration was 18 mg/mL. For comparison, a linear amylose sample (AS-1000, Nakano Vinegar, Aichi, Japan) was also used for the measurements. Chemical shifts of ^{13}C NMR spectra were measured in reference to internal acetone ($\delta = 33.02$).

Small-angle X-ray scattering.—Small-angle X-ray scattering (SAXS) was observed from aqueous solutions of CA21 at 25 °C. The concentrations of the solutions measured were, 3.1, 9.3, and 18.7 mg/mL. The SAXS experiments were performed with the SAXES (small-angle X-ray scattering equipment for solutions) optics installed at BL10C in the Photon Factory, Tsukuba, Japan [7,8] according to the method previously reported [5]. The observed range of the magnitude of the scattering vectors $\boldsymbol{q}$ was from 2.50×10^{-2} Å^{-1} to $\boldsymbol{q} = 0.5$ Å^{-1}, which is equivalent to the Bragg spacings from 251 Å to 12.6 Å. A flat cell ($1 \times 0.5 \times 0.1$ cm^3) fitted with a pair of quartz windows (20 μm thick) was centered in the incident X-ray beam. The cell was thermostated by circulating water of a constant temperature through the cell holder. The scattered intensities were corrected for the variation of the incident X-ray flux by monitoring the beam with an ionizing chamber placed in front of the thermostated sample holder. The excess scattering intensities were calculated by subtracting the scattering intensities of water from those of the solutions. The particle scattering function, $P(\boldsymbol{q})$, is defined by $P(\boldsymbol{q}) = I(\boldsymbol{q})/I(0)$, where $I(\boldsymbol{q})$ is the scattered intensity at a scattering vector $\boldsymbol{q}$ and $I(0)$ is the corresponding intensity extrapolated to $\boldsymbol{q} = 0$.

Molecular modeling based on the Monte Carlo method.—(1 → 4)-α-D-Glucan chains were generated according to the disaccharide conformational energy map by the Monte Carlo method as reported previously [9,10]. The energy map for α-maltose used in this study has been refined so as to yield the chain dimension and scattering function observed for

Table 1
Geometrical parameters for generating various initial model structures in Fig. 7a to i

Code	Form	Radius (Å)	D_z (Å/res)	Loop size
a	3-turn single	2.971	3.543	
b	3-turn single	3.658	2.971	
c	3-turn single	4.05	2.77	
d	3-turn single	4.6	2.6	
e	2-turn single	5.1	3.3	
f	2-turn single	6.0492	2.718	
g	double	5.185	2.33	8+9
h	double	2.989	3.43	8+7
i	double	5.185	2.33	8+7

Table 2
Assignments[a] of signals in ^{13}C NMR spectra of cycloamylose and linear amylose

Samples	C-1	C-2	C-3	C-4	C-5	C-6
CA21	102.40	74.41	75.97	79.92	73.95	63.22
Amylose	102.44	74.33	76.12	79.66	73.98	63.22
Amylose[b] (Low dp)	102.4	74.4	76.1	80.2	74.1	63.5

[a]Chemical shifts in ppm relative to internal acetone (δ 33.02).
[b]Taken from Ref. [28].

malto-oligosaccharides and amylose in solution. The torsion angles ϕ and are defined as $\phi = \theta$[H-1,C-1, O, C-4′] and $\psi = \theta$[C-1,O, C-4′, H-4′], respectively. The calculation takes into account the nonbonded van der Waals contributions and electrostatic contributions due to partial charges, where the bond angle τ at the glycosidic oxygen was fixed to 118°. The occurrence probability for a given ϕ and ψ pair was obtained by normalizing the Boltzmann factor associated with each ϕ and ψ pair by the sum of all such Boltzmann factors [9,10]. The normalized radial distribution function $W_x(r)$ of the end-to-end distance r was evaluated from 5000 chains of length x by counting the number of chains whose end-to-end distances were found to be in the interval dr between r and $r + dr$.

Among the generated chains in the Monte Carlo sample for a given dp, those with an end-to-end distance less than 1.5 Å were considered to be the examples of cyclic (1 → 4)-α-D-glucans. The ensemble of linear (1 → 4)-α-D-glucan chains used for computing the averages was composed of 500 chains. All glucose O-6 atoms were fixed in a gauche-trans (gt) conformation with torsion angle θ[O-5, C-5, C-6, O-6] and the torsion angle θ[C-4, C-5, C-6, O-6].

Molecular modeling based on a wire model.— According to the method previously described [2], we also constructed several helical models for CA21. For a single helical model, we formed a single helical pathway of a radius ρ and k turns deformed around a

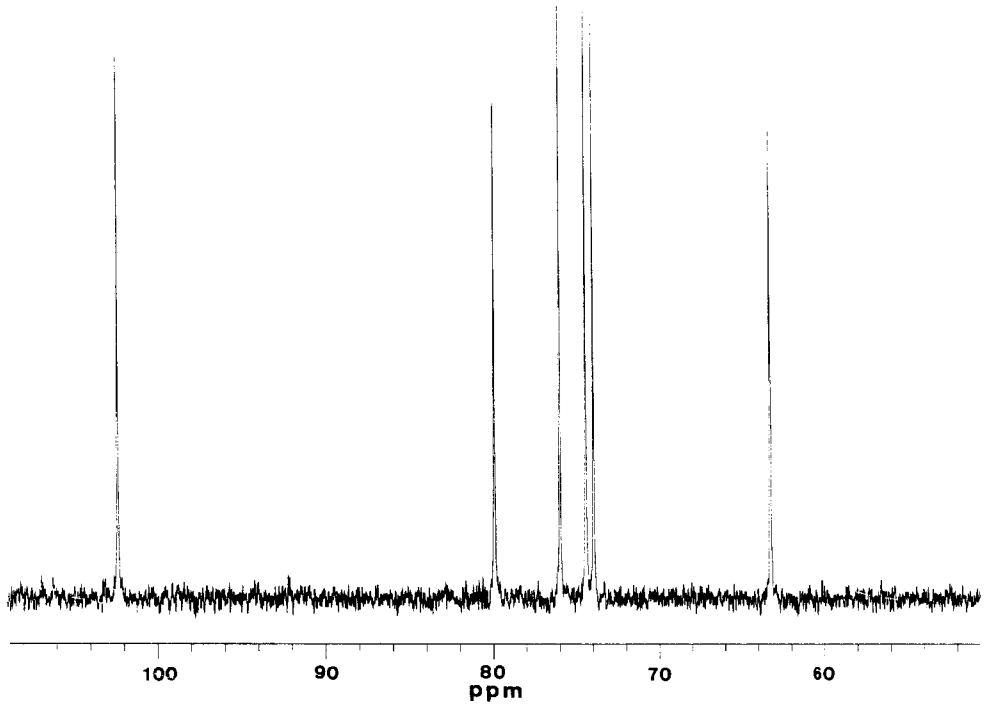

Fig. 1. ^{13}C NMR spectrum of CA21 in deuterium oxide at 27.5 °C.

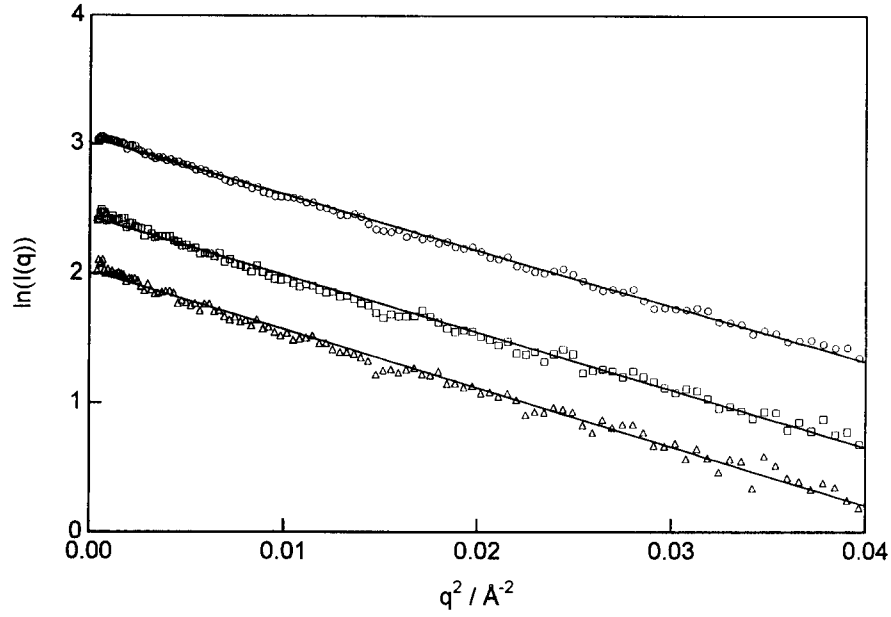

Fig. 2. Guinier plots of SAXS for CA21 in water at 25 °C at three different concentrations: (△) 3.1, (□) 9.3, (○) 18.7 mg/mL.

large circle of a radius R, assuming $2\pi R = nD_z$, where D_z is the axial rise per residue and n = dp. In the previous report, we constructed the single-helical structures with two sets of parameters: (ρ, D_z) = (5.185 Å, 2.33 Å) and (2.989 Å, 3.545 Å). However, these two sets were found to be insufficient for modeling CA21. Indeed the single-helical model with $\rho = 5.185$ Å caused severe steric repulsion at the center of the toroid. Instead, we have varied ρ in the range between 3 and 6 Å, and chosen D_z in such a way that two ends almost meet. Having established the positions of the oxygens, the rigid glucose units were then placed such that the V-shape of the C–O–C glycosidic linkage was aligned with the curvature of the string. A slight mismatch in the chain ends was compensated by distributing equally into each unit.

For the double helical model, we assumed two types of an antiparallel double helix: one has a radius

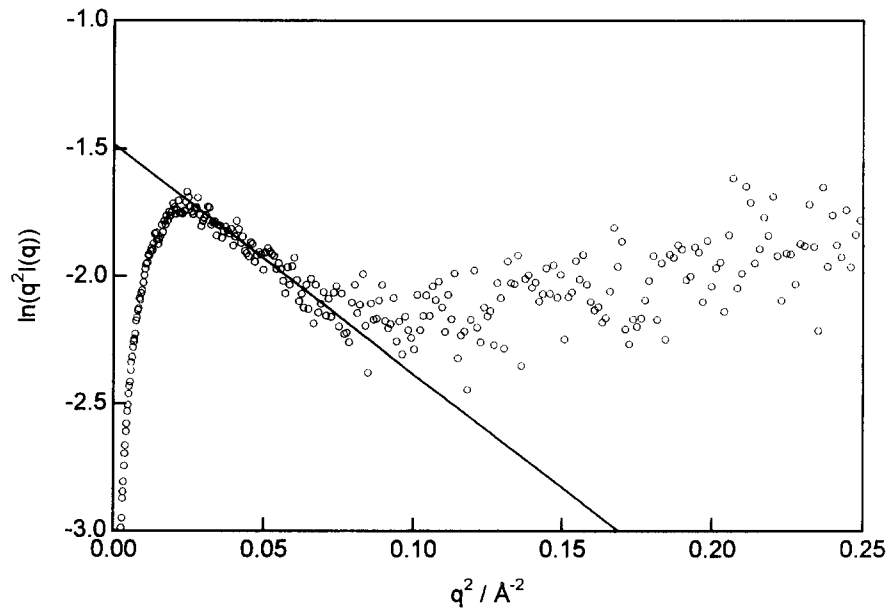

Fig. 3. Plot of $q^2P(q)$ vs. q for CA21 in water at 25 °C at 18.7 mg/mL. The solid line was obtained by linear regression of the data in the range of $q = 0.025 - 0.07$ Å, and its slope was used to calculate the thickness T in Eq. (5).

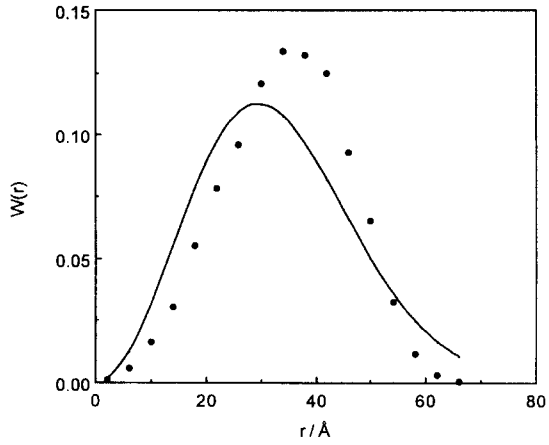

Fig. 4. Normalized radial distribution function $W_x(r)$ for (1 → 4)-α-D-glucan with dp = 21 (· · ·). The Monte Carlo sample contained 5000 chains and distance intervals, dr = 2.0 Å. Solid lines are Gaussian distribution functions for chains with $\langle r^2 \rangle_0$ values equal to those computed from the Monte Carlo samples.

5.1 Å, a helix pitch 18.6 Å and eight residues per turn except for several terminal residues, while the other has a radius 2.989 Å, a helix pitch 21.2 Å and six residues per turn [11,12]. A simple continuous elastic wire model was introduced to assist the atomic modeling of foldbacks. This model is assumed to be composed of a regular arrangement of glycosidic oxygens along a smoothly varying elastic string. In a manner similar to that suggested for a closed circular DNA [13], we represented the string by a B-spline curve and determined the conformation of the foldbacks by minimizing the elastic energy. The local elastic energy takes a minimum in the regular helical form with the above radius and pitch. Glucose units were placed as described above. The number of glucose residues of the terminal loops was varied around eight. Table 1 summarizes geometrical parameters used for single and double helical models of CA21.

The strain in the structures thus built was removed by energy minimization in vacuum, for which a simple distance-dependent dielectric constant was used to mimic the electrostatic shielding of surrounding water.

Molecular dynamics simulation.—Molecular dynamics simulations of CA21 were carried out in a manner as previously described [2]. A CA21 molecule was immersed in a large water sphere of a radius about 25 Å (1999 water molecules), and simulations were carried out for at least 100 ps with a timestep of 2 fs at 300 K. The results beyond 100 ps were used for the calculation of the scattering function. Molecular dynamics calculation employed a homemade program (NEC), where a new, fast multipole method was incorporated to calculate accurately long-range electrostatic interactions [14,15]. All bond lengths were constrained by applying the SHAKE procedure with a tolerance of 10^{-10} [16]. GROMOS parameters [17,18] and TIP3P water model [19] were used, and the temperature was controlled by the Nose–Hoover scheme [20,21]. Escape of water from the sphere was prevented by applying a weak central force beyond 1.5 Å separation [2]. To examine the influence of the force field used, some of the simulations were also carried out with the AMBER/GLYCAM field [22–24] with a timestep of 0.5 fs without bond length constraints. This field was developed on the *ab initio*

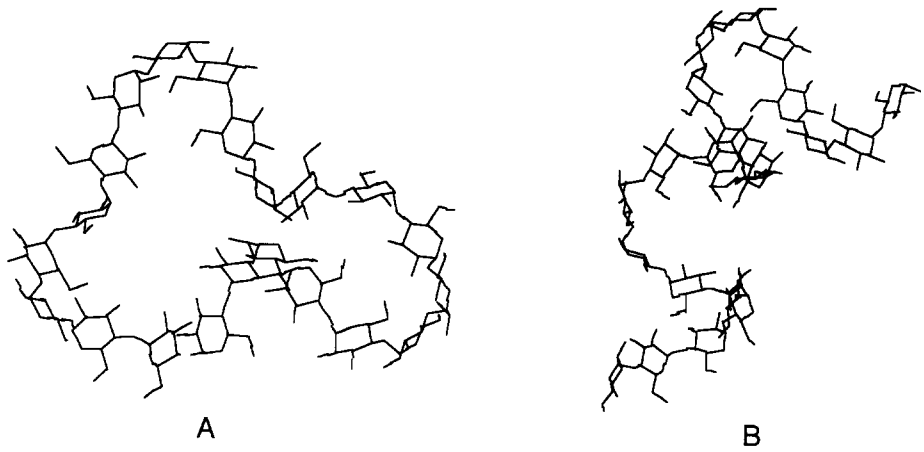

Fig. 5. Representative linear (1 → 4)-α-D-glucan chain with r = 1.5 Å (A) and with r = 32.5 Å (B) which is close to the mean value for the corresponding 500 chains. The hydrogen atoms are not shown. The O-6 atoms are affixed to pyranose rings at gt conformation. Model (A) was considered to be an example of CA21 and used for further calculations.

HF/6-31G* basis, and accounts for the exo-anomeric torsional terms, whereas the GROMOS field does not, as pointed out by Ott and Meyer [25]. NEC SX-3 and EWS4800 computers were used for the calculation.

Calculation of scattering function.—The scattering profile $I(q)$ was calculated as a function of the magnitude of the scattering vector q from the atomic coordinates of the molecular model chains according to the Debye formula [26,27]:

$$I(q) = \sum_{i=1}^{n} f_i^2 g_i^2(q) + 2\sum_{i=1}^{n-1}\sum_{j=i+1}^{n} f_i f_j g_i(q) g_j(q) \frac{\sin d_{ij}q}{d_{ij}q} \quad (1)$$

$$q = (4\pi/\lambda)\sin(\theta/2) \quad (2)$$

where, f_i is an atomic scattering factor, and d_{ij} is the distance between the ith and jth atoms, and λ and θ are the wavelength of the incident beam and the scattering angle, respectively. The form factor for a single atom $g_i(q)$ is assumed to be given by the form factor of a sphere with the radius equivalent to the van der Waals radius of the ith atom as

$$g_i(q) = \frac{3[\sin(R_i q) - (R_i q)\cos(R_i q)]}{(R_i q)^3} \quad (3)$$

with R_i being the van der Waals radius of the ith atom. The radii of carbon and oxygen atoms are taken to be 1.67 Å and 1.50 Å, respectively. The simulated scattering profiles are directly compared with those observed by SAXS by normalizing with respect to the scattered intensity at the zero angle.

All calculations of scattering function were performed on an IBM Power station 220.

3. Results and discussion

NMR spectra.—Fig. 1 shows a ^{13}C NMR spectrum of CA21 in deuterium oxide. Only six carbon signals are observed, suggesting that the glucose residues of CA21 are equivalent on the NMR time scale. Assignments of the ^{13}C NMR spectrum of CA21 are summarized in Table 2, together with those for linear amyloses. These assignments are based on the reported values obtained for a linear amylose in deuterium oxide [28]. It is seen that the chemical shifts of CA 21 are very similar to those of the corresponding resonances of linear amylose. The measurement of ^{13}C–^{1}H COSY two-dimensional NMR also supported this finding (data not shown). Thus, the glucose residues of CA are conformationally equivalent on the NMR time scale and the local

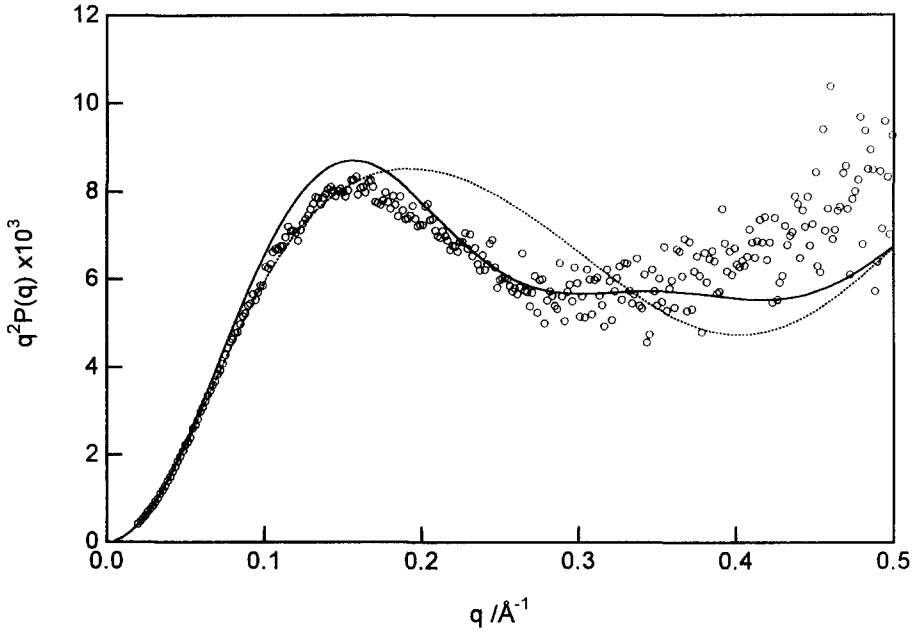

Fig. 6. Kratky plots of SAXS experimental data along with the theoretical scattering profiles calculated from a pseudo-cyclic chain (————), and from an ensemble of 500 Monte Carlo glucan chains (— —).

conformational characteristics are expected to be similar in CA as well as in linear amylose in aqueous solution.

Chain dimension evaluated by SAXS.—Fig. 2 shows the Guinier plots of CA21 in water at three concentrations. The radius of gyration R_G was evaluated from the initial slope of the Guinier plots ln $I(q)$ vs. q^2 according to the Guinier approximation [27], which reads:

$$I(q) \propto \exp(-R_G^2 q^2/3) \quad (4)$$

R_G is evaluated as 11.5, 11.4, and 11.3 Å for the polymer concentrations of 3.1, 9.3, and 18.7 mg/mL, respectively, indicating that R_G is virtually independent of CA concentration.

The thickness T of CA was evaluated, assuming to be represented by a flat disk, according to the Guinier plots for thickness [27]

$$q^2 I_{\text{flatdisk}}(q) \propto \exp(-q^2 T^2/12)/A \quad (5)$$

where A denotes the cross-sectional area. The plot of $\ln(q^2 I(q))$ vs. q^2 is shown in Fig. 3. From the slope of the linear relation in the range of $q = 0.025 - 0.07$ Å^{-1}, the thickness was estimated to be 10.4 Å. Compared with the results on cyclosophoran having dp 21 [5], the value of R_G for CA is larger by 2 Å than cyclosophoran, but the value of the thickness is similar.

Simulation using molecular models.—Fig. 4 shows the radial distribution function of the end-to-end distance $r, W_x(r)$, for linear (1 → 4)-α-D-glucan chains (dp = 21). The solid line in the figure represents

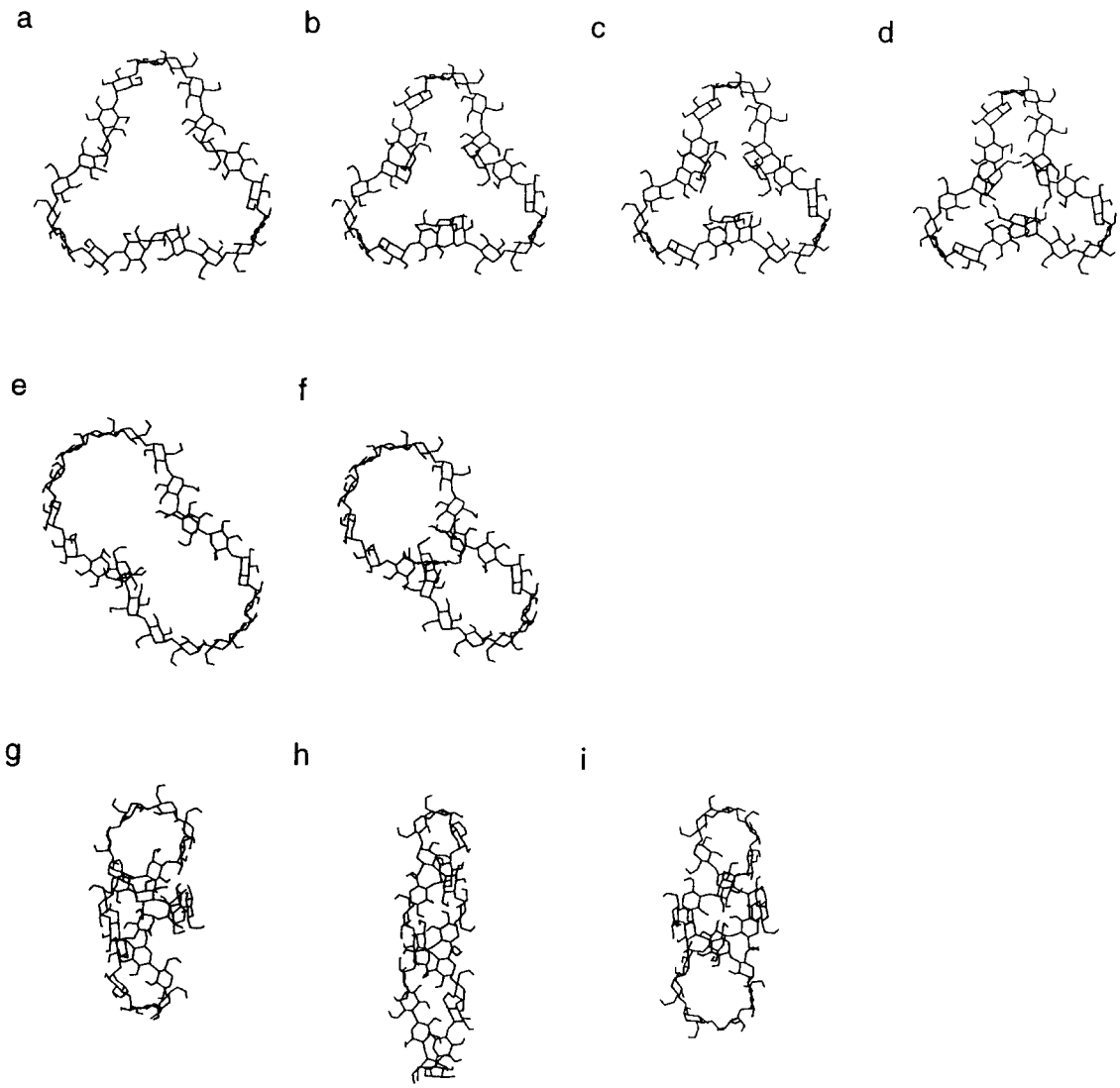

Fig. 7. Various initial conformations of CA21. Conformations a–i are generated with the corresponding parameter codes given in Table 1.

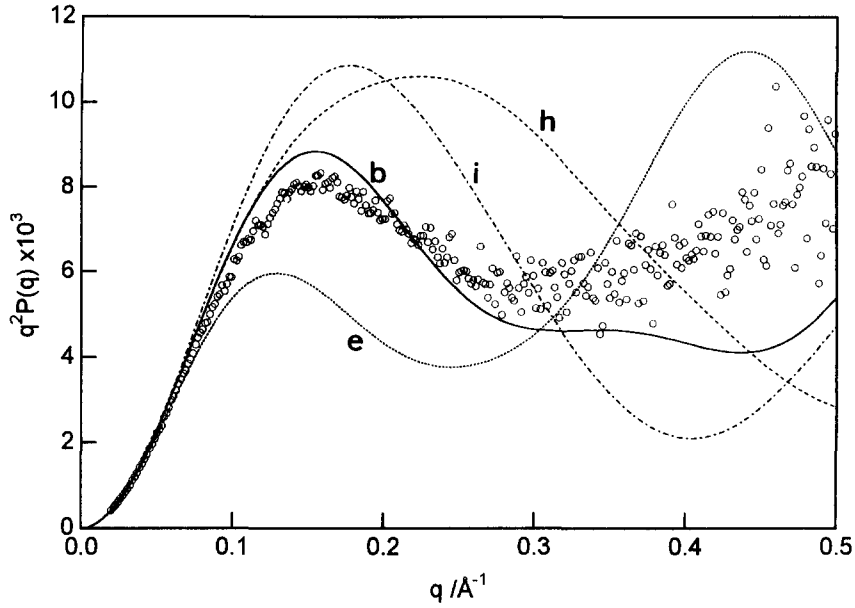

Fig. 8. Scattering profiles of some molecular models (b, e, h, and i) in Fig. 7. This figure includes the experimental profile (○).

the Gaussian distribution function corresponding to the chains with a mean-square end-to-end distance $< r^2 >$ equal to that computed from the Monte Carlo samples. It is seen that $W_x(r)$ for the chains with dp = 21 can not be represented by a Gaussian distribution function. We have collected 'pseudo-cyclic glucans' from Monte Carlo generated linear (1 → 4)-α-D-glucan chains whose ends are separated by less than 1.5 Å, and a representative model chain was selected from the collection of pseudo-cyclic glucans based on the consistency of the calculated and observed R_G (Fig. 5). Here R_G was calculated directly from the atomic coordinates of the Monte Carlo sample chains. Although this model chain is not closed covalently to form a ring, the scattering profile calculated from the atomic coordinates agree reasonably with that observed by SAXS as shown in Fig. 6. The figure also includes the scattering profile averaged over an ensemble of 500 Monte Carlo linear glucan chains.

The experimental SAXS profile is further compared with those calculated from several models. Fig. 7 shows the conformational characteristics of the chain models. Among the models, the most satisfactory result is obtained from a three-turn single helical chain. The two double-helix models yield less satisfactory results with respect to the scattering profile (Fig. 8). Although the radii of gyration evaluated from the double helix chains are in good agreement with the observed values by SAXS, the deviation in scattering profile becomes apparent even at $q = 0.1$ Å^{-1}.

Although the three-turn single helical model simulates well the observed scattering profile in the range of $q < 0.3$ Å^{-1}, the deviation from the experimental profile becomes serious at larger q. This deviation can be reduced by introducing a smaller apparent scattering unit in Eq. (3), but its physical significance cannot be explained explicitly at this stage. It should be noted that a similar deviation at large q has been observed for the simulation of cyclosophoran [5], and linear oligosaccharides [3,4]. The deviation is speculated as being due to a specific interaction between solvent and sugar residues [29–31]. Refinement of the simulation incorporating the solute–solvent interaction is a matter for further investigation.

Molecular dynamics in water.—For each conformation shown in Fig. 7, the molecular dynamics

Fig. 9. Superposition of the scattering profiles calculated for 12 consecutive 100, 130, 160, 180, 190, 220, 250, 280, 310, 340, 370, 400 ps atomic coordinate sets from the dynamic model of CA21 (model b), whose snapshots are shown in (b). Broken line represents the scattering profile obtained with the AMBER/GLYCAM field at 250 ps.

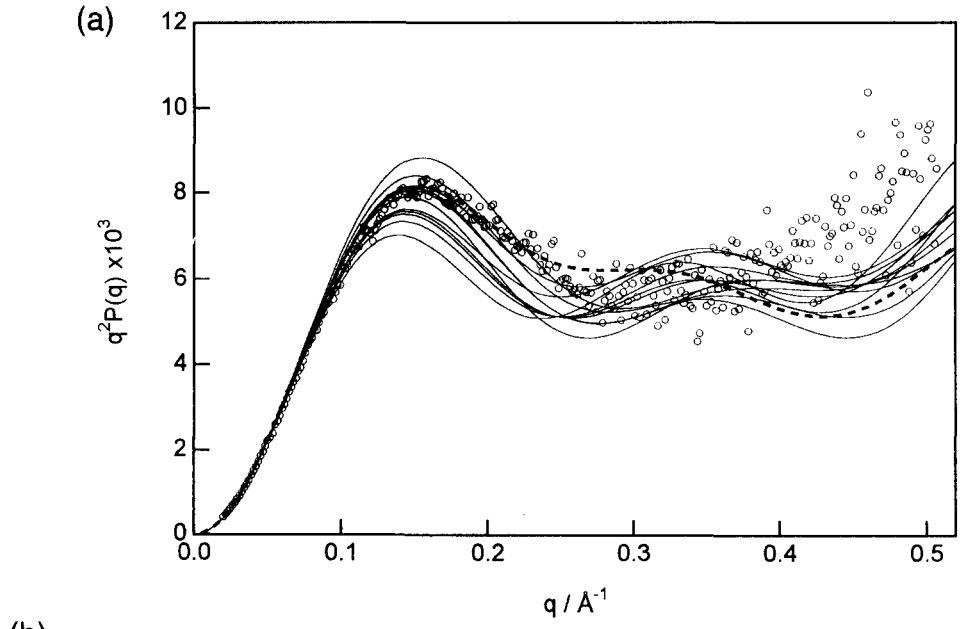
(a)
12
10
8
6
4
2
0
$q^2P(q) \times 10^3$
0.0
0.1
0.2
0.3
0.4
0.5
q / Å^{-1}

(b)

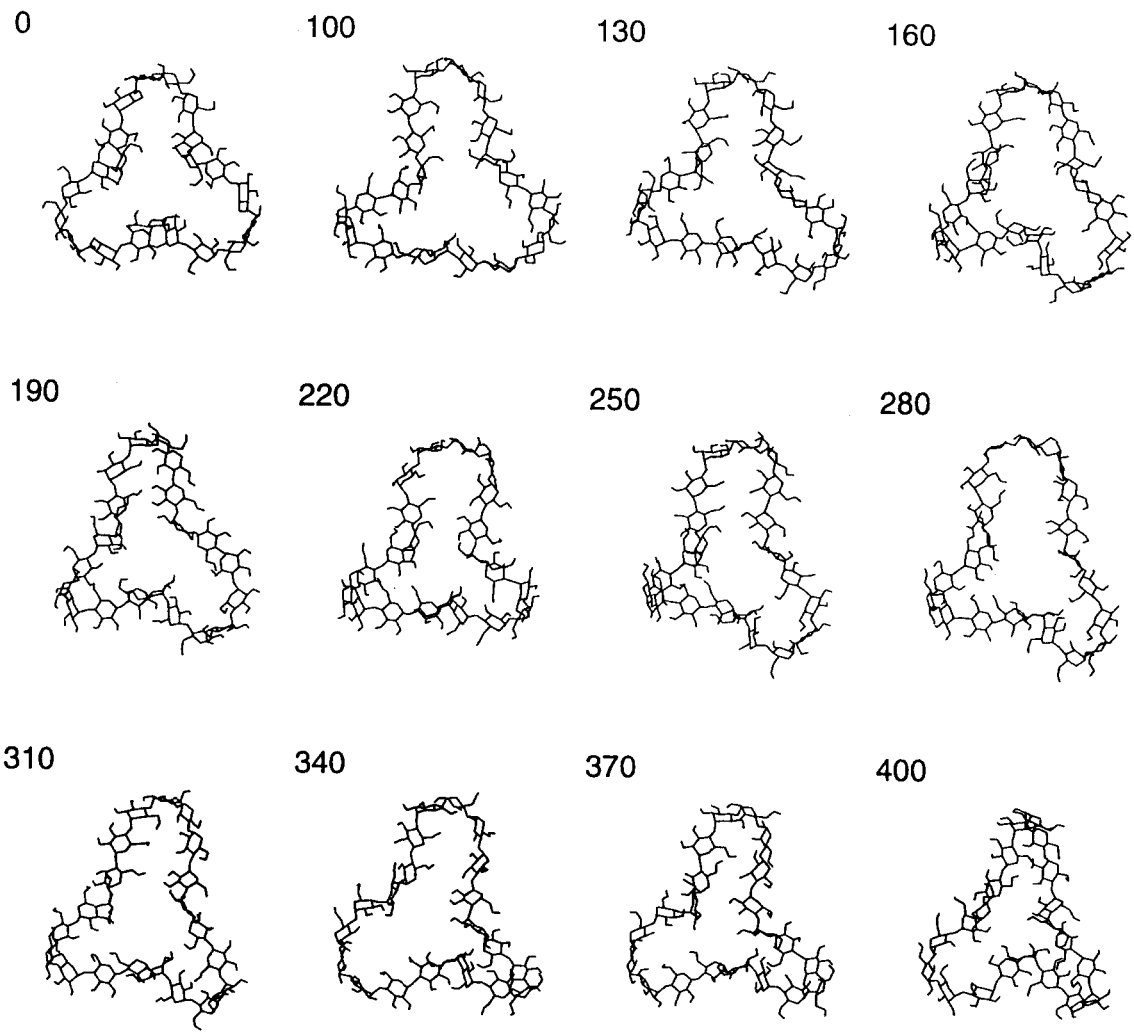
0
100
130
160
190
220
250
280
310
340
370
400

simulation was carried out for at least 100 ps. For the best-fit model b, the simulation was further extended to 400 ps. Fig. 9a shows the scattering profiles between 100 to 400 ps at 30 ps intervals. It is seen that the scattering profile fluctuates, reflecting a conformational change of the molecule with time. During this period, R_G fluctuates in the range of 0.7 Å around its mean. The scattering profile of an initial regular structure deformed slightly as time proceeds, as seen from Fig. 8 (curve b) and Fig. 9b. This slight deformation may be regarded as reflecting the process of randomization of the regular helical conformation. However, it is important to note that the essential feature of the starting scattering profile is maintained during the simulation.

One may wonder whether the scattering profile of

Table 3
Molecular dynamics simulation results on R_G for CA21 at 300 K

Code	R_G (Å)		Simulation time (ps)
	Initial	Final	
a	13.206	11.565	120
b	11.616	11.571	180
		11.065	400
c	10.993	11.810	180
d	10.553	10.776	210
e	13.611	11.255	180
f	12.273	11.170	150
g	10.472	9.934[a]	120
h	11.732	10.879	100
i	10.249	8.702	220

[a]Number of water molecules is 2960.

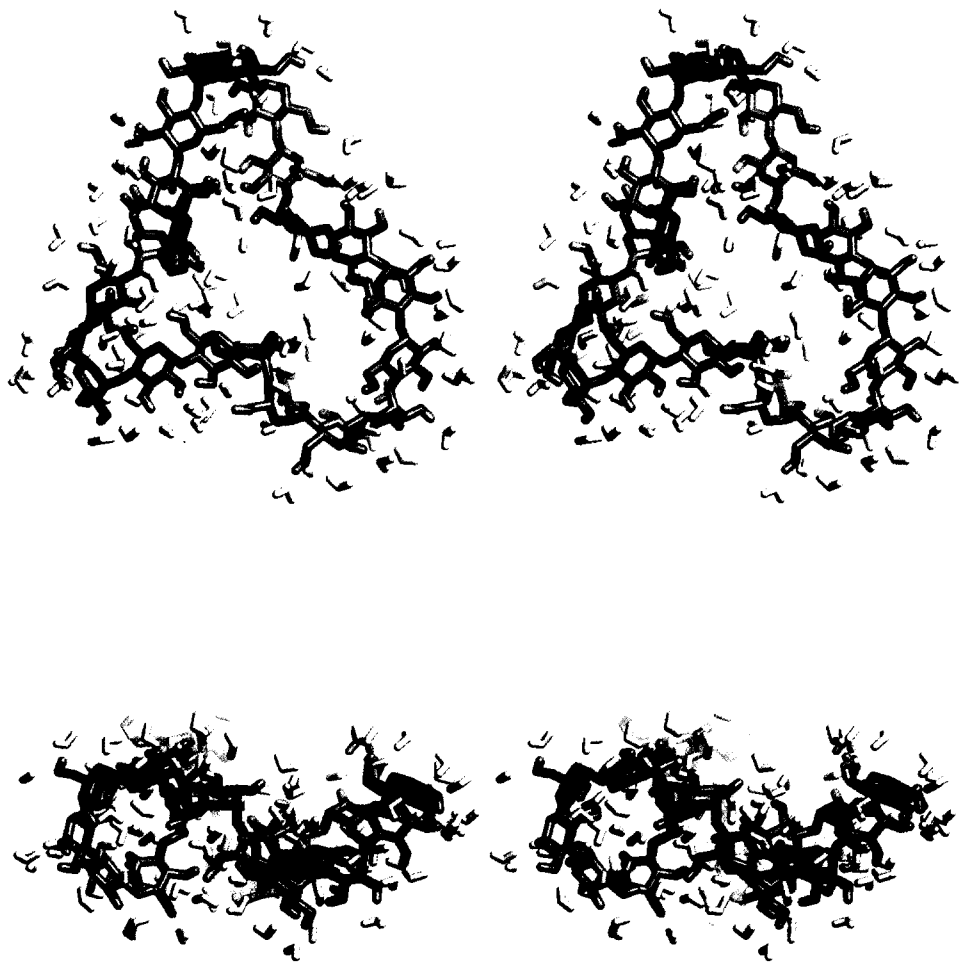

Fig. 10. Stereoview of the snapshot of CA21 with hydrogen-bonded water molecules. This view was obtained by 180 ps molecular dynamic simulation in water at 300 K. C, O, and H of CA21 are shown in gray, red, and blue, respectively, and the water molecules are shown in yellow. Right and left views are separated by 36 Å along the horizontal direction.

the double-helical models might approach the observed profile by simulation. However, each double-helical model shrinks considerably during simulation, decreasing its R_G by about 1–2 Å as seen from Table 3. As a result, the agreement became even worse than that with the starting conformation with respect to both R_G and the scattering profile. It may be helpful to note that a general trend is that the first peak of the scattering profile is more enhanced with decreasing R_G.

Fig. 10 shows a CA21 molecule where water molecules are incorporated and hydrogen bonding is introduced. Here water molecules are regarded as being hydrogen-bonded if the following three conditions are satisfied: (1) the donor–acceptor distance is smaller than 3.4 Å, (2) the hydrogen-acceptor distance is smaller than 2.4 Å, and (3) the donor–H-acceptor angle is larger than 150° [32]. The number of such water molecules is about 100 (96 for this snapshot), indicating that approximately 4.6 water–glucose hydrogen bonds are formed per glucose unit. Intramolecular hydrogen bonds were also observed for about 30% of 21 consecutive O-2 and O-3′ pairs. Its frequency is intermediate between simulated results for cyclodextrins (nearly 100%) [18] and maltose (3%) [25]. Two to four water molecules were observed in the inner cavity, although the counting is somewhat arbitrary for this molecule.

In the MD simulations of macromolecules, one always encounters the problem that the simulated results may depend on the initial conformation and the force field used. Four three-turn structures in Fig. 7a–d are considered as initial conformations in the present case. When the GROMOS field is used, the simulations starting from (a)–(c) gave a similar conformation with nearly the same R_G of about 11.5 Å at 100–180 ps, whereas the simulation starting from (d) gave a more compact conformation, yielding about 1 Å smaller R_G. Thus, there is indeed an initial conformation dependence, but the comparison with the SAXS observation strongly suggests that the three-turn structure as shown in Fig. 5A and Fig. 7b is close to reality.

In order to examine the influence of force fields on the present result, we repeated some of the calculations with the AMBER/GLYCAM field recently developed by Woods [23] and Woods et al. [24]. The scattering profile for model b is also included in Fig. 9a at 250 ps. When GLYCAM field was used, the single helical structure was again favored.

Acknowledgements

This work was performed under the approval of the Photon Factory Advisory Committee (proposal No. 94G-291).

References

[1] T. Takaha, M. Yanase, H. Takata, S. Okada, and S.M. Smith, *J. Biol. Chem.*, 271 (1996) 2902–2908.
[2] J. Shimada, S. Handa, H. Kaneko, and T. Takada, *Macromolecules*, 29 (1996) 6408–6422.
[3] M. Mimura, H. Urakawa, K. Kajiwara, S. Kitamura, and K. Takeo, *Macromol. Symp.*, 99 (1995) 43–55.
[4] S. Kitamura, T. Minami, Y. Nakamura, H. Isuda, H. Kobayashi, M. Mimura, H. Urakawa, K. Kajiwara, and S. Ohno, *J. Mol. Struct., (THEOCHEM)*, 395 (1997) 425–435.
[5] M. Mimura, S. Kitamura, S. Gotoh, K. Takeo, H. Urakawa, and K. Kajiwara, *Carbohydr. Res.*, 289 (1996) 25–37.
[6] W.S. York, J.U. Thomsen, and B. Meyer, *Carbohydr. Res.*, 248 (1993) 55–80.
[7] K. Kajiwara and Y. Hiragi, *Structure Analysis by Small-Angle X-ray Scattering*, in H. Saisho and Y. Gohshi (Eds.), *Applications of Synchrotron Radiation to Materials Analysis*, Elsevier, Tokyo, 1996, pp. 353–404.
[8] T. Ueki, Y, Hiragi, Y. Izumi, H. Tagawa, M. Kataoka, Y. Muroga, T. Matsushita, and Y. Amemiya, *Photon Factory Activity Report*, 1 (1983) V7, V29, V170.
[9] R.C. Jordan, D.A. Brant, and A. Cesaro, *Biopolymers*, 17 (1978) 2617–2632.
[10] S. Kitamura, T. Okamoto, Y. Nakata, T. Hayashi, and T. Kuge, *Biopolymers*, 26 (1987) 537–548.
[11] W. Hinrichs, W., G. Buettner, M. Steifa, Ch. Betzel, V. Zabel, B. Pfannemueller, and W. Saenger, *Science*, 238 (1987), 205–208.
[12] W. Schulz, H. Sklenar, W. Hinrichs, and W. Saenger, *Biopolymers*, 33 (1993), 363–375.
[13] M.-H. Hao and W. Olson, *J. Biomol. Struct. Dyn.*, 7 (1989) 661–692.
[14] L. Greengard, *Science*, 265 (1994) 909–914.
[15] J. Shimada, H. Kaneko, and T. Takada, *J. Comput. Chem.*, 14 (1993) 867–878; 15 (1994) 28–43.
[16] M.P. Allen and D.J. Tildesley, *Computer Simulation of Liquids*, Oxford Univ. Press, Oxford, UK, 1987.
[17] J.E.H. Koehler, W. Saenger, and W.F. van Gunsteren, *Eur. Biophys. J.*, 16 (1987) 197–210.
[18] J.E.H. Koehler, W. Saenger, and W.F. van Gunsteren, *J. Mol. Biol.*, 203 (1987) 241–250.
[19] W.L. Jorgensen and J. Tirado-Rives, *J. Am. Chem. Soc.*, 110 (1988), 1657–1661.
[20] S. Nose, *J. Chem. Phys.*, 81 (1984) 511–519.
[21] W.G. Hoover, *Phys. Rev. A*, 31 (1985) 1695–1697.

[22] S.J. Weiner, P.A. Kollman, D.A. Case, U.C. Singh, C. Ghio, G. Alagona, S. Profeta Jr, and P. Weiner, *J. Am. Chem. Soc.*, 106 (1984) 765–784.
[23] R.J. Woods, *The Application of Molecular Modeling Techniques to the Determination of Oligosaccharide Solution Conformation*, in K.B. Lipkowitz and D.B. Boyd (Eds.), *Reviews in Computational Chemistry*, VCH Publ., New York, 1996, Vol. 9, pp. 129–165.
[24] R.J. Woods, R.A. Dwek, C.J. Edge, and B. Fraser-Reid, *J. Phys. Chem.*, 99 (1995) 3832–3846.
[25] K.-H. Ott and B. Meyer, *Carbohydr Res.*, 281 (1996) 11–34.
[26] O. Glatter, *Acta Phys. Austr.*, 52 (1980) 243–256.
[27] G. Porod, *General Theory*, in O. Glatter and O. Kratky (Eds.), *Small Angle X-ray Scattering*, Academic Press, London, 1982, pp. 17–51.
[28] A. Heyraud, M. Rinaudo, M. Vignon, and M. Vincendon, *Biopolymers*, 18 (1979) 167–185.
[29] M.Y. Pavlov and B.A. Fedorov, *Biopolymers*, 22 (1983) 1507–1522.
[30] C.A. Pickover and D.M. Engelman, *Biopolymers*, 21 (1982) 817–831.
[31] A.S. Hyman, *Macromolecules*, 8 (1975) 849–857.
[32] W.F. van Gunsteren and M. Karplus, *Macromolecules*, 15 (1982) 1528–1544.